Australian Government
Department of Defence
Defence Science and
Technology Organisation

A Detailed Study of Sonar Tomographic Imaging

H.T. Tran [1], ***B. Nguyen*** [2], ***R. Melino*** [1], ***and S. Wood*** [2]

[1] **Electronic Warfare and Radar Division**
[2] **Maritime Operations Division**

Defence Science and Technology Organisation

DSTO–RR–0394

ABSTRACT

Sonar tomography is a technique to obtain a two-dimensional image of an underwater object using a sequence of one-dimensional images, or 'projections', of the object of interest. We discuss sonar tomography in a detailed manner and compare the performance of two important 'back-projection algorithms' commonly used in tomography. The two processing techniques are applied to the imaging of relatively small underwater objects using high sonar frequencies, making use of simulated and experimental data. We also discuss system requirements, as well as the similarities and differences with radar applications. Ultimately, the performance of this underwater object imaging technique is determined by the availability of sufficiently high resolution projections and/or sufficient coverage in object aspect.

Published by

DSTO Defence Science and Technology Organisation
PO Box 1500
Edinburgh, South Australia 5111, Australia

Telephone: 1300 DEFENCE
Facsimile: (08) 7389 6567

AR No. 015–647
May, 2013

APPROVED FOR PUBLIC RELEASE

A Detailed Study of Sonar Tomographic Imaging

Executive Summary

For decades, sonar has been used for the detection, location, and classification of underwater objects. Modern diesel submarines radiate very little acoustic noise, making their detection by conventional passive systems, which rely on the analysis of submarine-radiated acoustic noise, very difficult. This has led to a renewed interest in the use of active sonar systems to detect submarines. However the effective use of an active sonar system in shallow and/or cluttered littoral environments requires an ability to distinguish between active sonar returns ('echoes') from submarines and those from other objects in the environment ('false alarms'). One approach to classifying active sonar returns uses the backscattered sonar echoes as projection information for object classification using two dimensional acoustic tomography.

In the two-dimensional reflection tomography method presented, the object is rotated while being ensonified by short sonar pulses. For each aspect angle of the object, the scattered sonar pulse is recorded as a function of time, or distance through the object. A collection of such projections from a wide enough range of aspect angle is input to a Back Projection Algorithm (BPA) to form an object image. As the data is collected radially about the axis of rotation, one computation method computes an inverse Fourier transform using polar coordinates. Another method interpolates the scattering data into rectangular coordinates, then performs a two-dimensional inverse Fourier transform (2DIFT). In both cases it is important to remove any relative movement between the transducer and axis of rotation, prior to tomographic processing.

While sampling rate and duration of the pulse determines down-range (or radial) resolution, the angular step size between projections and a sufficient total angular coverage determine cross-range (or angular) resolution, with a formula presented to calculate the optimal step size. This represents a compromise between image resolution and computational cost.

The theory of two dimensional tomography is not directly applicable to sonar reflections for a number of reasons, including that the scattering mechanism is reflective rather than transmissive, parts of the object can scatter like a highly directional antenna causing high-amplitude specular reflections or flashes, and parts of the object can obscure scattering from more distant parts causing missing data. To alleviate such undesirable effects, we use a scaling factor to attenuate the specular reflections, and average projections spaced 180° apart to reduce the obscuration.

Tomographic imaging results with both simulated and experimental data are presented. The simulated projections are obtained from a numerical scattering model based on the Helmholtz-Kirchhoff integrals. In one simulation the transmitted signal consists of two cycles, giving an impulse-like signal. The second simulation uses a longer transmit pulse, as used in the experimental measurements. The experimental data is collected in a water tank, in which three objects are ensonified, namely a solid granite cylinder, a brass tube, and a scale model of a generic submarine.

Sharp tomographic images are obtained with the short-pulsed simulated data; with the longer pulsed simulated data the images are not quite as sharp. It is concluded

that polar BPA processing requires an appropriate choice of attenuation factor to reduce the effect of the specular reflections, while for the 2DIFT BPA approach the degrading effect from these reflections is negligible, and so the attenuation factor is not necessary. This may be heuristically explained by noting that the polar BPA achieves integration by accumulating the projections sequentially which can be abruptly and strongly affected by specular reflections, while the 2DIFT BPA achieves integration after all projections have been collected and across the two rectangular dimensions. For the same reasons, it is also noted that the polar BPA approach tends to highlight the flat and point-like features of the object better, while the 2DIFT BPA approach tends to highlight the more curved or cone-like shapes better.

The experimentally obtained projections show scattering from the ends and sides of the object, the suspension points, and multiple scattering near beam aspects. This last source adds scattering that can obscure some of the geometric features shown in the image. For the granite cylinder the 2DIFT BPA approach performs more robustly, producing a 'cleaner' image, while the polar BPA approach can produce strong and clear object features, but requires careful tailoring of the attenuation factor. For the brass tube it is not obvious which approach performs better. The polar BPA approach gives stronger returns along the object body, but introduces more background artifacts. The images of the scaled generic submarine are complex, with both approaches performing equally.

Finally, images are produced from the short-pulsed simulated data, but using only a half or quarter cycle of rotation. Although not quite as sharp as for a full cycle of rotation, the images with a half cycle of rotation are similar. However, when using only a quarter cycle of rotation, only half of the object is imaged.

Contents

Figures

Glossary

2DIFT - 2-Dimensional Inverse Fourier Transform

BPA - Back Projection Algorithm

FT - Fourier Transform

IFT - Inverse FT

ISAR - Inverse Synthetic Aperture Radar

LFM - Linear Frequency Modulation

PSF - Point Spread Function

THIS PAGE IS INTENTIONALLY BLANK

1 Introduction

Imaging an underwater object with active sonar provides a potential basis for sonar target classification, regardless of whether the classification system is fully automatic or a human-in-the-loop system. This work explores the use of tomography as a useful and effective technique in sonar imaging applications.

The use of two dimensional sonar tomography for the imaging of underwater objects is not new. Ferguson and Wyber [1, 2] have reviewed its mathematical theory in a systematic manner and applied it to sonar data. Before these recent works, there were also earlier reports from Doisy [3] and Pidsley *et al.* [4] on the subject. Nevertheless, we discuss here the subject in a more detailed manner, compare the performances of two important 'back-projection algorithms' commonly used in tomography and apply the theory to the imaging of relatively small scale underwater objects using high-frequency sonar pulses, based on laboratory experimental and simulated data. We also discuss system requirements, the importance of 'pre-processing', which ultimately determines the best tomographic image quality possible with a given system, as well as the similarities and differences with radar applications.

Tomography is basically a mathematical technique of reconstructing a two-dimensional function from one-dimensional projections of the function at different aspect angles. This involves the Radon transform and back-projection algorithms to reconstruct the original function. In X-ray tomography, which is usually referred to as Computer Aided Tomography (CAT), the projections are density measurements. In radar tomography, they are range profiles, either in the down-range or cross-range directions. In sonar tomography, they can only be down-range profiles, here referred to as (down-range) *projections*, due to a lack of useful Doppler modulations.

At sonar frequencies, signal bandwidth is often such that the projections obtained with many sonar systems do not contain a great deal of information about the object, except for a very small number of scattering centres of the object. Hence, despite the fact that projections may be available over very small steps of the object aspect angle, a large overall coverage of aspect angle may be necessary for tomography to synthesise a reasonable image of the object. This is a significant difference when compared to the radar counterpart problem of inverse synthetic aperture radar (ISAR), where a great deal of information (possible with the availability of relatively high bandwidth) can be captured in each projection and only a small[1] coverage of aspect angle is required to produce a useful image of an object.

The main sections of the current work are as follows. Section 2 presents a brief review of the basic theory, and discusses issues such as scattering effects expected in sonar, image resolution and system requirements while Section 3 summarises and discusses the results of our study.

One important assumption we emphasise at the outset is the need to compensate for any translational motion (of the centre of rotation) of an object, before the application of tomographic processing.

[1] Typically less than 10°.

2 Sonar Tomography

This section briefly summarises the theory of two-dimensional reflection tomography, and discusses the advantages and disadvantages of two different approaches of the so-called 'Back Projection Algorithm' (BPA), as well as issues arising from its application to the problem of sonar imaging. Specific attention will be given to image resolution limits from a theoretical standpoint, system requirements and issues from real measurements and phenomenology.

2.1 The Basic Theory

The essence of tomographic imaging is the BPA [5, 6, 7, 8], and has also been discussed recently in the context of sonar tomography in [1, 2]. The theory can be formulated as a general two-dimensional (2D) Fourier analysis technique as follows. For a 2D real-valued function $q(x, y)$, as shown in Figure 1, the projection $p_\theta(r)$ along a line through the origin at angle θ, which is also called the Radon Transform, may be defined as

$$p_\theta(r) = \int_{-\infty}^{\infty} \int_{-\infty}^{\infty} q(x, y)\, \delta(x \cos\theta + y \sin\theta - r)\, dx\, dy. \tag{1}$$

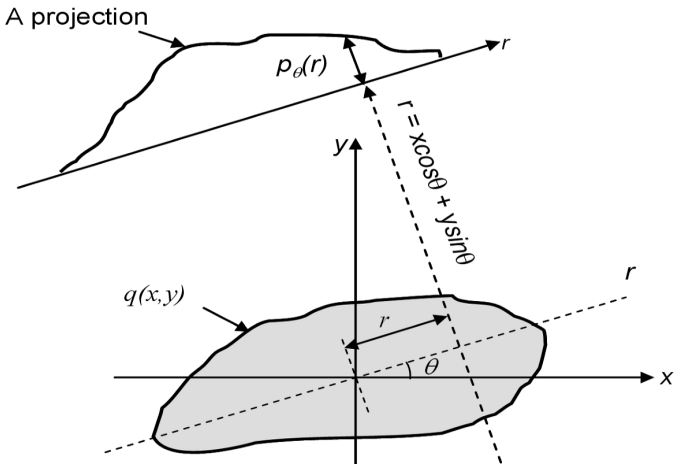

Figure 1: *Projection of a 2D function, $q(x, y)$.*

It can be readily verified that the spatial Fourier transform $P_\theta(f_r)$ of $p_\theta(r)$, with spatial frequency in the r-dimension denoted as f_r, is a slice at angle θ, $Q_\theta(f_x, f_y)$, of the 2D Fourier transform of $q(x, y)$, i.e.,

$$\begin{aligned} P_\theta(f_r) &= \int_{r=-\infty}^{\infty} p_\theta(r)\, e^{-i2\pi f_r r}\, dr & (2) \\ &= Q_\theta(f_x, f_y). & (3) \end{aligned}$$

Here,

$$f_x = f_r \cos\theta, \quad f_y = f_r \sin\theta$$

are the spatial frequency components in the x and y-dimensions along the slice at angle θ. This is the so-called *Projection-Slice Theorem*.

Once Q is constructed from many such slices over a sufficient range of aspect angles θ, $q(x, y)$ can be obtained from a 2D inverse transform; this is generally called the Back Projection Algorithm (BPA). Furthermore, noting that $df_x\, df_y = f_r\, df_r\, d\theta$, the 2D inverse Fourier transform (2DIFT) on Q can be done in rectangular coordinates (f_x, f_y), or in polar coordinates (θ, f_r) (see [5] for example):

$$q(x,y) = \int_{-\infty}^{\infty}\int_{-\infty}^{\infty} Q_\theta(f_x, f_y)\, e^{i2\pi(x\, f_x + y\, f_y)}\, df_x\, df_y \tag{4}$$

$$= \int_0^{\pi} \mathcal{F}^{-1}\left\{|f_r|\, P_\theta(f_r)\right\}_{(x\cos\theta + y\sin\theta)}\, d\theta. \tag{5}$$

The subscript $(x\cos\theta + y\sin\theta)$ in the above equation means the inverse Fourier transform (IFT), denoted by $\mathcal{F}^{-1}$, is calculated at $r = x\cos\theta + y\sin\theta$.

Note also that it requires only half a cycle of rotation of the object to fully sample (in angle θ) the 2D frequency plane.

2.1.1 The BPA in rectangular coordinates

In rectangular coordinates, as expressed in (4), an interpolation process is required to obtain estimates of $Q_\theta(f_x, f_y)$ on a regular rectangular grid, from measurements $P_\theta(f_r)$ in polar coordinates, before the 2DIFT can be performed, as illustrated in Figure 2. Indeed, in most sonar and radar applications, only measurements in the form of either down-range projections or cross-range projections are available, both of which are in polar coordinates. The interpolation requirement means that, if the 2DIFT approach is utilised, measurements need to be made at all representative aspect angles of the target. Interpolation errors inevitably become larger for larger magnitudes of the spatial frequency f_r. In this work, we will use the spline interpolation technique as implemented in the MATLAB's *interp2* function.

The spacing and extent of the rectangular grid points are parameters to be chosen, guided by object features of interest. In general, image resolution and coverage may increase with finer spacing and larger extent of the rectangular grid, with an increasingly higher computational cost. However, information content is limited by the original bandwidth of the signal, hence there is a point where a finer spacing of the rectangular grid points will not yield any better image resolution. The most effective selection of these parameters should thus be based on object features of interest. If object features close to the centre of rotation are more desirable in the final image, then a finer spacing and a small extent may be more appropriate. On the other hand, if features further away from the centre are more desirable, then a coarser spacing and a larger extent may be a more suitable choice.

2.1.2 The BPA in polar coordinates

In polar coordinates, as expressed in (5), the integral can be numerically approximated as a summation of many 'corrugated' surfaces at a range of aspect angles θ from 0 to

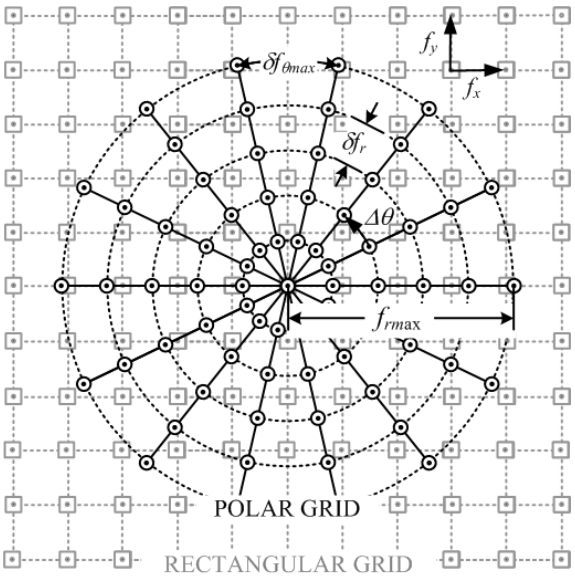

Figure 2: *Polar grid (for measurements) and rectangular grid (for 2DIFT BPA). (Adapted from [1])*

π, scaled by a finite angular step size $\delta\theta$. Each of such surfaces is determined by the projection $p_\theta(r)$, and is parametrized by the radial spatial coordinate r and 'projected' in the (x, y) plane along tangential direction (perpendicular to the radial direction) such that $x\cos\theta + y\sin\theta = r$ at each value of r. To put it in another way, the 'corrugated' surfaces arise from the projection of the integrand in (5), which is a function of r, in the tangential direction.

There are two known 'sub-methods' to calculate the integral in (5), as has been discussed extensively elsewhere. The reader is again referred to [5], for example. It suffices here to mention that, for the first method, called the Filter Back-Projection method, the IFT in (5) is computed directly (and numerically necessarily), while for the second method, called the Convolution Back-Projection method, the convolution theorem is applied to compute the IFT.

2.1.3 Discussion

As noted before, both BPA approaches require half a cycle of rotation of the object to fully sample the frequency plane. A possible advantage in utilising the polar coordinate approach as compared to the 2DIFT approach is that, numerically, it may perform better when the object projection data is available in less than half a cycle of the aspect angle. Such a scenario can be quite common in practical applications where a target's maneuvering and its change of aspect angle relative to the sonar is limited.

However, a disadvantage of the polar coordinate approach comes from its sensitivity to transient but strong specular reflections, or 'flashes', at particular aspect angles. Because the BPA integral (5) is computed as a summation of 'corrugated surface' terms, each of which is determined by a projection at angle θ, a specular reflection can cause a particular term to strongly dominate the sum, giving rise to spurious effects in the resulting image.

Measures to alleviate this problem and further discussion on this point will be presented later in the Report.

2.2 Application to Sonar Imaging

In a complete system, any relative motion between the transducer and the centre of rotation of the object must be removed, or compensated for, prior to the stage of tomographic processing. Any error in this step would result in phase distortions and a blurring of the final image. In this work, only simulated or experimental data of translationally non-moving objects are used, hence translational motion compensation is not necessary and will not be mentioned further.

2.2.1 Image resolution

Assuming that the scattering from an object can be modelled as an ensemble of point scatterers, we now discuss what can be expected for image resolution limits from a general theoretical standpoint, given relevant system and scenario parameters.

There are three main factors which affect image resolution. The first is waveform bandwidth responsible for down-range (or radial) resolution. The second factor is effective aperture, or equivalently angle of rotation, responsible for cross-range (or azimuthal) resolution. The third factor is the effect of the so-called Point Spread Function (PSF) arising from the fact that in practice only a portion of the frequency space can be sampled, at finite sampling rates.[2]

Projections in sonar imaging applications are most often measured in down-range, employing a linear frequency-modulated (LFM) waveform and a pulse-length reduction technique. Hence down-range resolution limits are determined by performance of the pulse-length reduction processing. It is well known (see [9] for example) that the -3 dB pulse-length reduction is approximately

$$\delta t = \frac{1}{\delta f}, \tag{6}$$

independent of, and also normally shorter than, the normal pulse length. Here, $\delta f = f_2 - f_1$ is the difference between the final and initial frequencies of the frequency sweep, i.e. the bandwidth of the pulse. Note that $1/\delta f$ is the ideal LFM pulse-length reduction *without windowing* which is usually desired to suppress compression sidelobes. For typical requirements on sidelobe suppression, the actual reduction of pulse-length may be many times larger than the ideal δt.

The aim in pulse length reduction is to achieve an input signal whose duration is as short as practically possible and whose sidelobe levels are as low as possible, to allow for the best possible object resolution in range. In practice, however, the sonar system is not limited by peak transmit power constraints but has to avoid reverberation problems associated with long-duration transmit pulses. Pulse-length reduction itself is used as part of the signal generation by employing a Finite-Impulse-Response filter applied to the

[2]The point spread function may be regarded as including the second factor as a part of it.

LFM signal, the output of which is a narrow pulse to be amplified prior to transmission. The receive signal is then match-filtered with the transmit signal. This process will be discussed in more detail later in the report.

For cross-range resolution, the result usually quoted in Inverse Synthetic Aperture Radar (ISAR) literature (see [10] for example) is

$$\Delta x = \frac{\lambda}{2\phi}, \tag{7}$$

where λ is the mean wavelength of the transmitted signal, and ϕ is the total angle of rotation of the object for the data collection time interval. However, it must be noted that the validity of (7) is based on the assumption, among others, that the point scatterers (or scattering centres) in all projections remain in the same range bins during the integration interval, which is *not* the case here. Indeed, in our current problem, the total angle of rotation may be up to half a cycle of rotation or more, and scattering centres widely move across range bins, suggesting the necessity of using some other benchmark to set cross-range resolution. More discussion is included in Section 2.2.2.

The PSF is the 2DIFT of a domain setting function $W_\theta(f_r)$ which modifies (5) slightly as follows:

$$q(x,y) = \int_0^\pi \mathcal{F}^{-1}\left\{W_\theta(f_r)\,|f_r|\,P_\theta(f_r)\right\}_{(x\cos\theta + y\sin\theta)}\,d\theta, \tag{8}$$

in which $W_\theta(f_r)$ is non-zero and equals unity only over some domain $(f_r,\theta) \in D$. As is well known, the broader the domain D, the more focused the PSF becomes, resulting in finer resolution for an image.

2.2.2 System requirements

Suppose $SF_s = 2\,F_s/c$ denotes the spatial sampling frequency used in the projections, where F_s is the corresponding temporal sampling rate and c is the speed of sound in water, then the spatial sampling interval is simply $1/SF_s$ $(= c/2\,F_s)$. Furthermore, the discrete Fourier transform of length N of a projection is spanned in spatial frequency from $-SF_s/2$ to $+SF_s/2$, with a spatial frequency bin size of

$$\delta f_r = \frac{SF_s}{N}. \tag{9}$$

These parameters will help quantify system requirements for tomographic processing.

First SF_s should be just large enough to capture the largest spatial frequency (or 'level of object feature sharpness') of interest, and at the same time keep computational cost to a minimum. Other requirements for effective tomographic processing are driven mostly by the resolution that can be achieved for each projection, which depends on the available performance of pulse compression processing in the sonar system. Referring to Figure 2, it is apparent that a suitable choice of the angular stepsize $\Delta\theta$ between the projections is such that

$$\delta f_{\theta max} \approx 2\,\delta f_{ref}, \tag{10}$$

where δf_{ref} is the smallest *effective* radial frequency bin size of a projection which takes into account imperfections due to the pulse compression processing discussed above.[3] Let us denote the maximum useful radial frequency by f_{rmax}, which may be equal to or less than $SF_s/2$, then[4]

$$\Delta\theta \approx \frac{\delta f_{\theta max}}{f_{rmax}}. \tag{11}$$

An inspection of the available data should be adequate as a guide on setting the most effective choices for SF_s and δf_{ref}. Nevertheless, assuming that $\delta f_{ref} = \kappa\, \delta f_r$ (for some constant parameter $\kappa \geq 1$), and a chosen sampling rate such that $f_{rmax} = \nu\, (SF_s/2)$ (for some constant $\nu \leq 1$), then Equations (10) and (11) mean

$$\Delta\theta \approx \frac{2\kappa\, SF_s/N}{\nu\, SF_s/2} = \frac{4\kappa}{\nu\, N}. \tag{12}$$

An example of this approximate result will be given in Section 3.

2.2.3 Real scattering effects and measurements

Strictly speaking, the theory of 2D tomography as summarised in Section 2.1 does not exactly apply to sonar and radar scattering problems, because: (a) projections that can be obtained by sonar and radar measurements are not exactly the types described in Equation (1); (b) the scattering mechanism in these problems is reflective in nature, not transmissive; (c) certain components of an object may scatter incident waves like a highly directional antenna, causing high-amplitude specular reflections; and (d) obscuration effects in which only one side of the object is illuminated are quite likely.

Nevertheless, at least two workarounds can be usefully applied to make good use of the current theory. The first workaround is an *attenuation factor* designed to attenuate the specular reflections in the scattered signal, which occur when a flat component of the object is facing normal to the line of sight of the sonar. Indeed, curved wires and surfaces are compatible with the current theory and can be expected to be imaged more efficiently than straight wires and especially flat surfaces, as will be demonstrated later. Mathematically, the workaround is here effected by simply scaling each projection with a scalar factor of the form

$$A_\theta = 1 - A_{max} \exp\left\{ -\frac{(\hat{p}_\theta - \hat{p}_{max})^2}{\sigma^2} \right\}, \tag{13}$$

where A_{max} (ranging between 0 and 1) is the maximum attenuation level chosen, $\hat{p}_\theta$ is the max amplitude of the projection at angle θ, $\hat{p}_{max}$ the (global) maximum amplitude across the whole data set, and σ is a width term adjusted so that the attenuation is effectively applied only to the specular reflections. These parameters may be set for a particular scattering object upon an inspection of the received data. We have also found that this workaround is most useful for the polar BPA approach, in which the inverse Fourier transform is computed in polar coordinates in a cumulative manner, and the

[3] A conservative choice is $\delta f_{ref} = \delta f_r$; however, the most effective choice may require an inspection of the quality of the projections.

[4] Again, a conservative choice is $f_{rmax} = SF_s/2$.

sensitivity can be affected by the specular reflections. Refer to discussion in section 2.1.3. Indeed, as will be evident later in the Report, the 2DIFT BPA approach does not need this attenuation factor at all.

If *obscuration* were not present, and all scattering centres are isotropic (i.e. ideal point scatterers), and if the data is entirely free of errors associated with translational motion compensation, then the rotational motion means that (referring to Figure 1) a projection would repeat itself after a rotation of 180°, except for reverse look direction from the sonar transducer, i.e. $p_\theta(r) = p_{\theta+\pi}(-r)$. Thus, a second workaround that can be used to reduce obscuration effects is by the approximation [1]

$$p^a_\theta(r) = 0.5\,\{p_\theta(r) + p_{\theta+\pi}(-r)\}. \tag{14}$$

Here, $p^a_\theta(r)$ denotes the 'averaged' projections to be used for tomographic processing. Strictly speaking, the factor 0.5 applies only in the absence of obscuration, i.e. when $p_\theta(r) = p_{\theta+\pi}(-r)$ is non-zero. However, since prior knowledge of the object and its exact rotational motion is generally not available, the 0.5 factor needs to be applied across the dataset, accepting a loss of -3 dB of the scattered signal when obscuration does occur. The approximation in (14) can also be interpreted as a measure to force the 'back lobes' of the scattering centres to be the same as their 'front lobes' - a step toward the ideal point scatterers assumption.

Finally, although a minimum of half a cycle of projection data is required for tomographic processing, the use of more than half a cycle of data (if available) and Equation (14) could help further improve the resulting image quality by enhancing the signal-to-noise ratio.

3 Results and Discussion

This section presents results and discussions for both simulated and experimental data. In terms of the required angular spacing $\Delta\theta$ between projections, the theoretical discussion in Section 2.2.2 can be applied as follows. For Equation (12), assuming $\kappa = 1$, our data is such that[5] $N = 326$ and $\nu \approx 0.75$, which leads to a value of about 0.94° for $\Delta\theta$. This requirement is roughly met by the currently available data: each data set consists of 361 projections, covering a full cycle from 0 to 360°, meaning the $\Delta\theta$ available from the data is approximately 1°.

3.1 Simulated Data

A numerical scattering computer model has been used to generate simulated datasets. This is a high-fidelity object scattering numerical model based on evaluating the Helmholtz-Kirchhoff (H-K) integral [11] for the object of interest. The surface of the object is modelled by a mesh of triangular facets, where the H-K integral is evaluated analytically for each

[5]This value for N, which is generally not a radix of 2, has been chosen based on the sampling rate, the decimation factor to minimise the data handling requirement, and the sonar pulse length to sufficiently sample the target in range.

triangular facet. The total scattered field from the object of interest is then obtained by a coherent summation of the scattered field from all the individual facets. The material properties of the target are encapsulated in the local reflection and transmission coefficients of the target. Additional complexities such as multiple transmissions, scattering from several layers, hidden surface removal and first-order multiple scattering have been found to be necessary inclusions to make the results realistic.

Results from the use of this scattering model and the back-projection algorithms described earlier to simulate the tomographic imaging of a relatively simple object are now discussed. The scattering object (designated 'BRS' and shown in Figures 8(a) and 3(a)) consisted of two, different diameter, cylinders joined by a truncated cone and fitted with hemispherical end caps. The total length of the object was 550 mm and the larger cylinder was 74 mm in diameter and 400 mm long. All elements were constructed from 0.3 mm thick brass.

Example 1

This example aims to demonstrate an 'upper limit' in terms of image resolution performance, when the sonar pulses employed are very short duration. A short 13.3 μs pulse (2 cycles) of 150 kHz carrier frequency was used as an impulse source which is directly input to the model to insonify the object. The projections generated by this model are shown in Figure 3(b), before application of the attenuation factor to reduce the specular reflections near angles 90° and 270° prior to further processing.

The tomographic imaging results from the first example are presented in Figures 3(c) and 3(d) for the polar BPA and 2DIFT BPA approaches respectively. Note that the attenuation factor in Equation (13) with $A_{max} = 0.9$ (corresponding to a maximum attenuation of -10 dB) and $\sigma = 5\,\hat{p}_{max}$ has been applied to reduce the specular reflections near angles 90° and 270°, for the polar BPA approach. (Refer to discussions in sections 2.1.3 and 2.2.3.)

Example 2

This example uses a 37 μs Linear Frequency Modulation (LFM) pulse, which was swept from 80 to 220 kHz as an input signal to the scattering model. A useful feature of the model is that real but undesirable physical effects such as multiple echoes can be controlled, thus allowing a better performance comparison between the polar and 2DIFT approaches of BPA. In this example, only two multiple echoes from within the object are simulated, minimizing the extent of noise-like signal components. The projections generated by this model are shown in Figure 4(a), again before application of the attenuation factor. What is immediately evident in the projections are the wider returns, the slightly more severe multiple echo effects near 90° and 270°, and a general reduction of detail when compared to the projections in Example 1.

Tomographic imaging results for this example are shown in Figures 4(b) and 4(c), using an attenuation factor with $A_{max} = 0.94$ (corresponding to a maximum attenuation of approximately -12 dB) and $\sigma = 5\,\hat{p}_{max}$ for the polar BPA processing. In this particular case, it can be observed that both BPA approaches feature the main scattering centres equally well. However, the polar BPA approach reconstructs the body and tail outline of the object slightly better, while the 2DIFT image highlights the more cone-shaped areas of

the model target, which is consistent with the outcome from the first example. Note that the stronger thickness of the outline of the shape seen in Figure 4(b) is directly related to the longer pulses (i.e. lower bandwidth) generated and transmitted by the system, significantly reducing the resolution of the images, compared to that in the first example. The broadening can also be seen in the projections in Figure 4(a).

Note that for both of the above examples, a full cycle of data has been used, which is twice the minimum required for tomographic processing. Nevertheless, they make a good case to compare the different requirements and performances of the two BPA approaches without too many of the non-ideal effects of the real world. The following points can be noted:

1. It is rather difficult to discuss image resolution in these examples. Nevertheless, for the short duration pulse on transmission in the first example, the apparent resolution achieved is better than 0.5 cm and clearly highlights all scattering centres of the model target. For the second example, resolution is degraded to about 1 cm.

2. The attenuation factor in Equation (13) proves to be a necessary workaround, for the polar BPA approach, without which spurious strong 'streaks' corresponding to the specular reflections near 90° and 270° would appear in the resulting image and could shadow (or desensitise) other object features that may be crucial for classification performance. Furthermore, if the object consists of multiple flat components with different scattering strengths, the choice of the attenuation factor may need some special tuning. However, this detailed tuning of the factor is outside the scope of the current Report.

   For the 2DIFT BPA approach, the degrading effect from the specular reflections is negligible, and the attenuation factor is not necessary. (For reasons, refer to discussions in sections 2.1.3 and 2.2.3)

3. As remarked earlier, curved surfaces of the object are well imaged, as evident by the nose-end in both images. However, the polar BPA approach tends to highlight the more flat and point-like features of the object better, such as the body, tail and junctions; while the 2DIFT BPA approach tends to highlight the more curved or cone-like shapes better, such as the nose-end, tail-end, and junction between the hull and tail.

4. Combining the two BPA approaches can potentially help to form a more complete picture of this object.

3.2 Experimental Data

3.2.1 The sonar measurement and processing system

Scattering experiments were conducted in a sonar laboratory that consisted of a large tank of water, acoustic transducers, and apparatus to rotate a test object (Figure 5).

Three objects of different acoustic properties and geometries were used as test objects. The first object was a solid granite cylinder with hemispherical end caps of dimensions

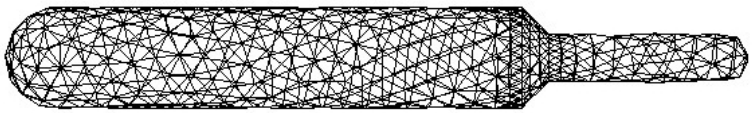

(a) Object model, in triangular meshes

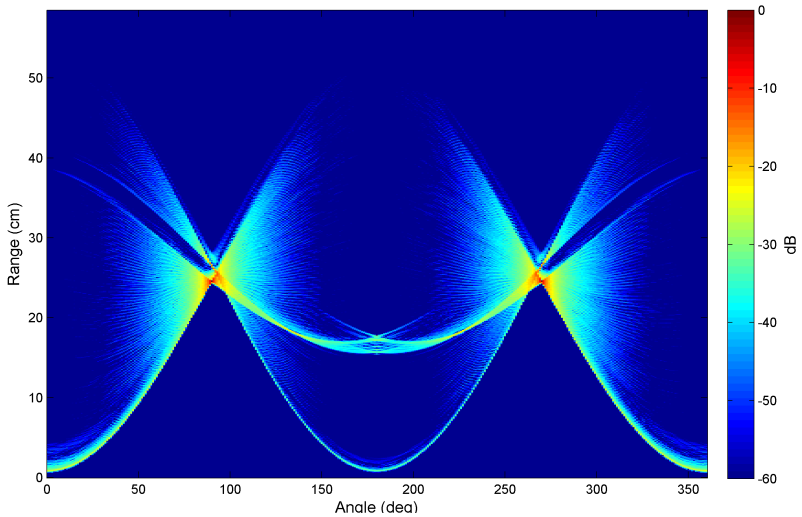

(b) Spectrogram (without attenuation factor applied)

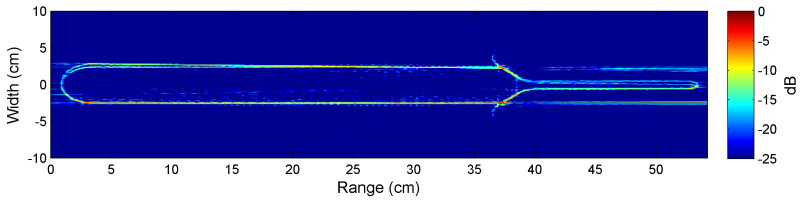

(c) Tomographic image - Polar BPA approach

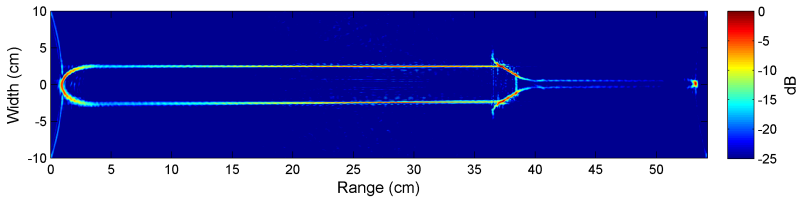

(d) Tomographic image - 2DIFT BPA approach

Figure 3: *Simulated results for the BRS object using a short duration pulse presented using both polar and 2DIFT BPA approaches.*

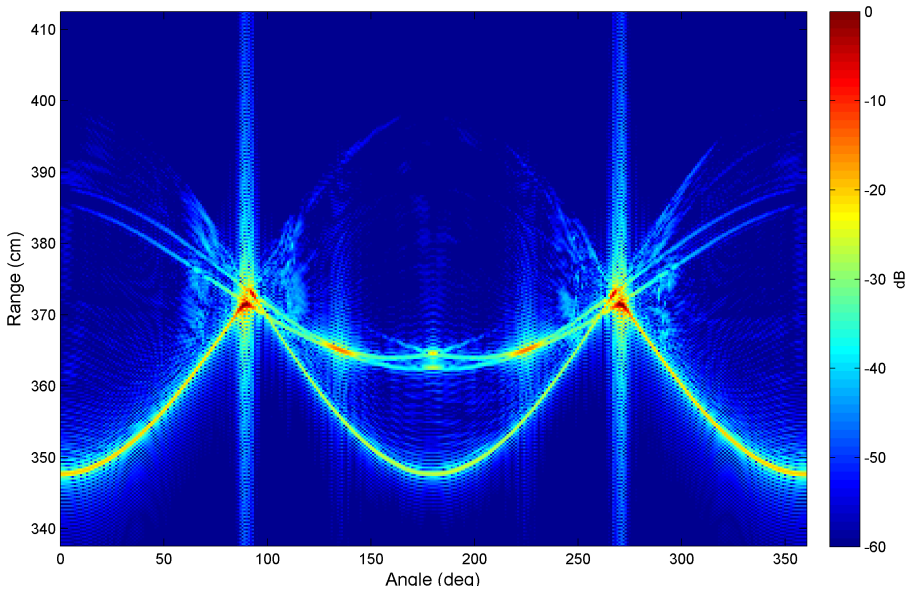

(a) Spectrogram (without attenuation factor applied)

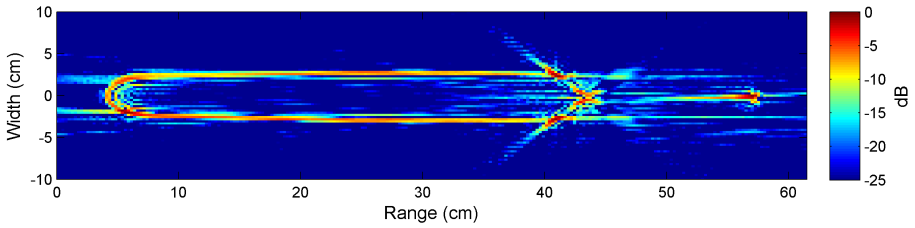

(b) Tomographic image - Polar BPA approach

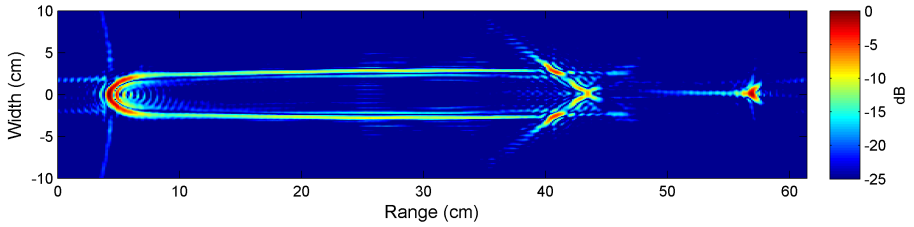

(c) Tomographic image - 2DIFT BPA approach

Figure 4: *Simulated results for the same object as in Figure 3, using the long duration transmit signal of the experimental system*

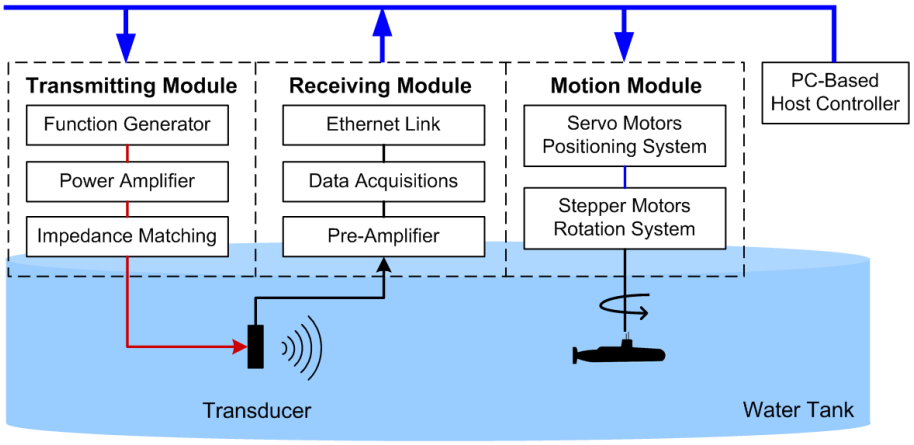

Figure 5: *A schematic diagram of sonar laboratory*

550 mm in length and 74 mm in diameter. It is denoted 'SG' and a photo of it is shown in Figure 7(a). The second object was a brass shape of dimensions as decribed in section 3.1 with a photo shown in Figure 8(a). The third object was a model of a generic submarine, 692 mm long with a hull diameter of 86.2 mm. It is constructed from 0.3 mm brass shim using a few simple shapes such as a hemispherical bow, cylindrical hull, cone-shaped tail and airfoil sale and control surfaces. It is denoted 'GenSub' and is shown in Figure 9(a).

Objects under test were rotated about their vertical axis in 1° increments using the motion module which was fully automated and controlled by the PC-based Host Controller as shown in Figure 5. The input signal generated by the Function Generator consisted of a band-limited up-sweep LFM pulse of duration 37 μs with a frequency spectrum between 80 and 220 kHz. The signal was transmitted repetitively with a 'ping interval' of 100 ms. A Butterworth filter of order 4 was used in the Function Generator to reduce the pulse-length of the transmit signal to minimize reverberation effects which can be particularly severe inside the relatively confined environment of the laboratory water tank. The scattered signal from each of the three objects, placed at a distance of 4 metres from the transducer was sampled at a rate of 6.25 MSa/s. To reduce transient and noise effects, at each aspect angle, multiple scattered pulses were averaged in the digitiser. Prior to tomographic processing, raw data was decimated by a factor of 4, to reduce the sample rate to 1.5625 MSa/s. Then matched filtering was carried out in the frequency domain by first applying a Blackman window to the scattered data from each aspect angle to reduce spectral leakage, followed by a multiplication of the transmit and receive complex spectra, and finally followed by an IFT back to the time domain.

Mathematically, the matched filter processing can be expressed as

$$p_\theta(t) = \mathcal{F}^{-1}\{S_{tx}(f)\, S_{rx}(f)\}, \tag{15}$$

where $p_\theta(t)$ is a compressed range profile, at aspect angle θ;

$$\begin{aligned} S_{tx}(f) &= \mathcal{F}\{w(t)\, s_{tx}(t)\}, \text{ and} \\ S_{rx}(f) &= \mathcal{F}\{w(t)\, s_{rx}(t)\}, \end{aligned}$$

are respectively the Fourier transforms of the transmit signal $s_{tx}(t)$ and the windowed

receive signal $s_{rx}(t)$, and $w(t)$ denotes a window function. Again, $\mathcal{F}^{-1}$ denotes the inverse Fourier transform.

Typical time domain plots of the transmitted signal and the matched filtered received signal are shown in Figure 6, in which the scattering object is the SG model target. A careful inspection of the matched filter output trace (Figure 6(b)) would reveal that the separate 'packets' correspond to separate scattering centres of the target. Matched filtering has helped in the suppression of the 'ripples' after the main pulse of the transmitted signal in (Figure 6(a)). It is important to use pulses which are as short as possible on transmit for optimum target image resolution. Using long pulses or packets with extensive oscillations on transmission may result in low resolution images, or images with 'contour lines'. Note that the matched filtering performed here has taken advantage of the availability of the waveform measured at the location of the target, to optimise the achievable SNR. However, in most practical situations, the matched filtering must be done with the transmitted signal.

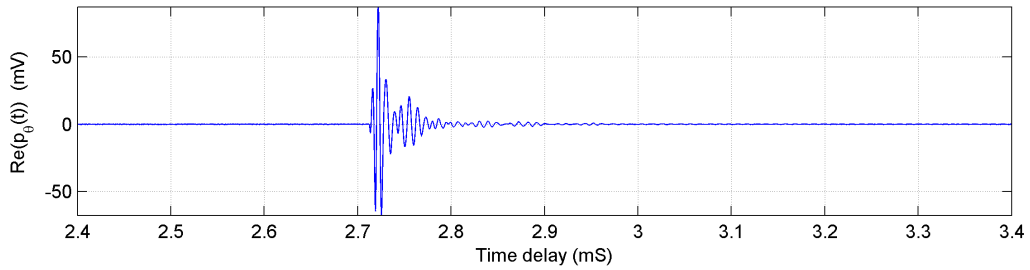

(a) Transmitted signal as measured at the target location

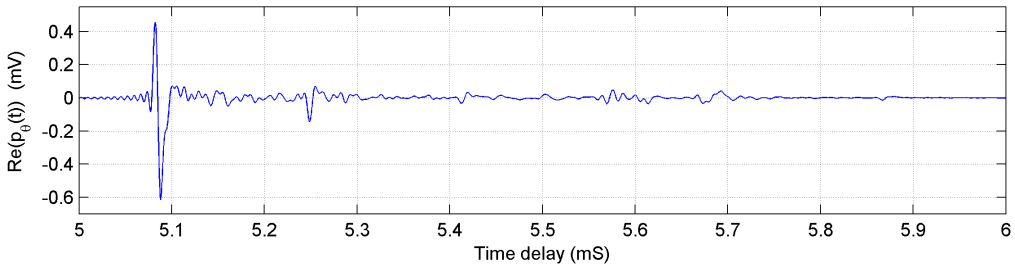

(b) Received signal after matched filtering, at target aspect of 10 deg

Figure 6: *Time series of a typical set of data*

For each received signal, at a particular angle, a projection is obtained indexed by the object's angular position. Over a range of angles, the resulting collection of such projections is here referred to as a 'spectrogram'.[6]

Imaging results are shown in Figures 7, 8 and 9. Again, image resolution achieved in these examples is limited primarily by the transmitted pulse width available with the

[6] Admittedly, the term 'spectrogram' is borrowed from the Doppler processing context, which is not the case here.

current system, while spurious features such as streaks are a result of non-ideal scattering characteristics of targets and the laboratory environment in the water tank which can not be totally compensated for prior to tomographic processing.

3.2.2 The SG object results

Figure 7(b) is the spectrogram for the SG object shown in Figure 7(a), with no attenuation factor applied, for the sake of clarity of various scattering phenomena involved. However, an attenuation factor A_θ with $\sigma = 5\hat{p}_{max}, A_{max} \approx 0.94$ is required for best tomographic imaging result with the polar BPA approach. One of the most striking features here are the multiple sonar echoes, labelled A, near the 'broadside' aspect angles of 90° and 270°. These are due to the excitation and re-radiation of helical compressional and shear waves along the cylindrical shell. The resonances occur when one round-trip phase increment along the shell circumference equals an integer multiple of 2π. These multiple echoes add interfering features in the background of the images shown in 7(c) and 7(d), especially 7(c) for the polar BPA image. Ideally, a pre-processing step to reduce such echoes should be in place if this sonar imaging technology is to be implemented in an operational system.

Other notable features in the signal include the sinusoidal traces of the echoes from the ends of the cylinder, labelled B & C, which are the echoes from the nose and tail of the object respectively. Also, the beam aspect reflection, labelled D, occurs at 90° and 270°. The magnitude of this reflection is approximately 30 dB greater than the off-beam aspect echoes. The dominance of this signal component can amplify the undesirable effects of the transient specular reflections and the accompanied high FT sidelobes in the form of streaks across the tomographic image produced using the polar approach. The effect is less pronounced, and in fact, negligible, in the tomographic image produced using the 2DIFT BPA approach in which the inverse Fourier transform is done in rectangular coordinates.

Another major feature in the received signal for this target are echoes that result from the four mounting hooks attached to the target, which are labelled E in Figure 7(b). As can be seen, continuous scattering from these hooks is quite prominent giving rise to the two clearly visible 'dots' in both tomographic images, where the hooks are located. Lastly, the low-intensity horizontal lines in Figure 7(b) are from other fixed features of the water tank, which also appear in the other data sets discussed later in this section.

Overall, the 2DIFT BPA approach performs more robustly for this target producing a 'cleaner' image, and requires no attenuation factor. On the other hand, the polar BPA approach can also produce strong and clear target features but requires a careful tailoring of the attenuation factor for best result.

3.2.3 The BRS object results

Figure 8(b) is the spectrogram for the BRS object shown in Figure 8(a), with $\sigma = 5\hat{p}_{max}, A_{max} \approx 0.94$ applied for the polar BPA processing. The spectrogram exhibits features similar to those described earlier for the SG object. However, the multiple echoes exist over a much wider sector of aspect angles around 90° and 270°, which add considerable interference to the resulting images in 8(c) and 8(d) in different ways.

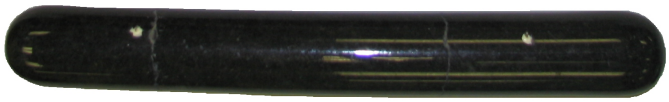

(a) A granite (SG) object

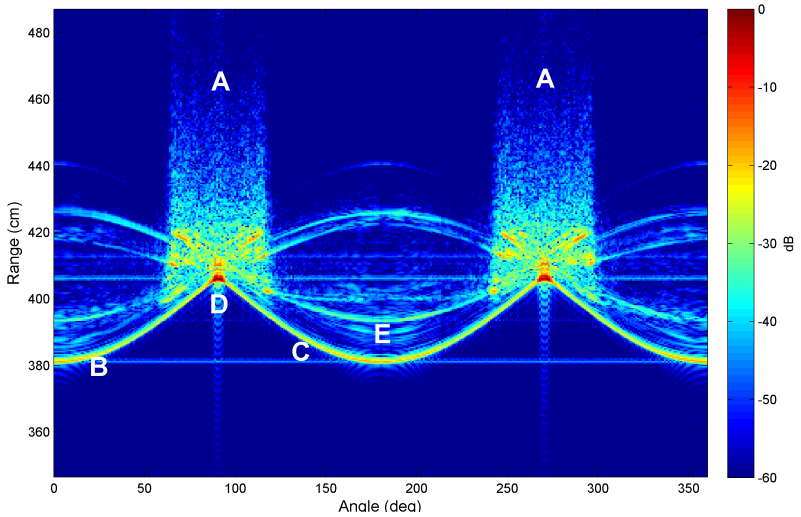

(b) Spectrogram (with no attenuation factor applied)

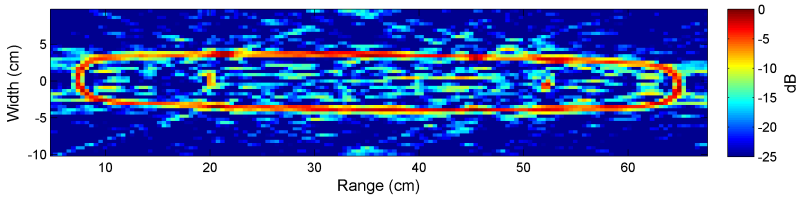

(c) Tomographic image - Polar BPA

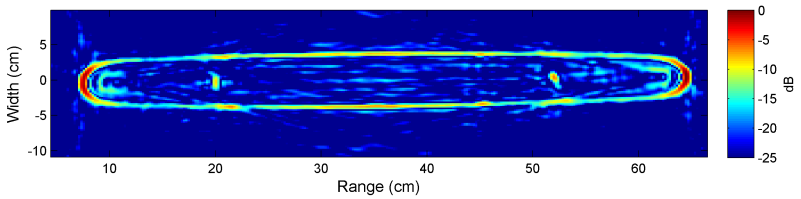

(d) Tomographic image - 2DIFT BPA

Figure 7: *Experimental results for the SG object*

(a) A brass shim (BRS) object

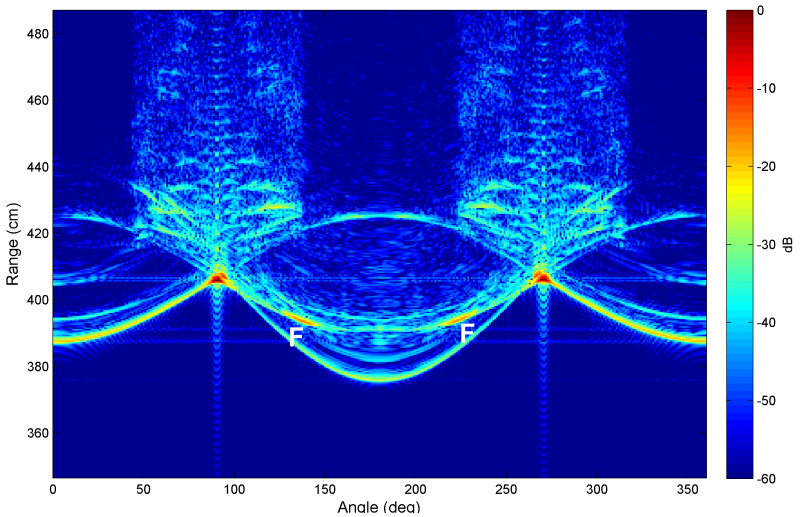

(b) Spectrogram with attenuation applied

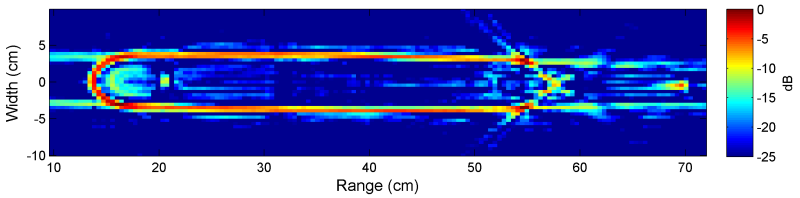

(c) Tomographic image - Polar BPA

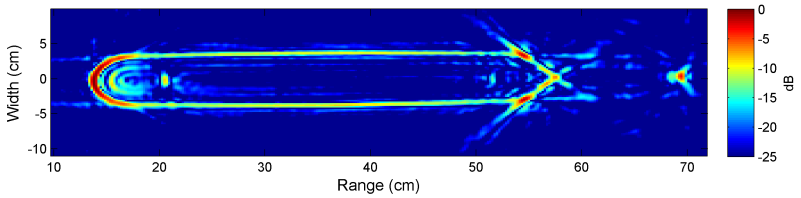

(d) Tomographic image - 2DIFT BPA

Figure 8: *Experimental results for the BRS object*

While there are more background artifacts in the image based on polar BPA, the features corresponding to the more pointed ends of the object are preserved. The returns along the object body are stronger; this however depends on the choice of the attenuation factor. Also, there is significant backscatter from the cone-shaped joint between the tail and the hull, labelled F, as can be seen in both tomographic images. The two hooks feature equally well in both images, though they could have appeared a little stronger in the polar BPA image if more attenuation was applied to suppress the component from the hull. The 'tail' section of the target features mostly only as a strong scatterer at the tip, which is the main scattering centre for the tail section.

Based on these results, it is not exactly obvious as to which of the two BPA approaches performs better - they appear to be complementary in terms of the target features highlighted.

3.2.4 The GenSub object results

Figure 9(b) is the spectrogram for the GenSub model shown in Figure 9(a), with $A_{max} \approx 0.99$ (-20 dB) and $\sigma = 5\hat{\rho}_{max}$ applied for the polar BPA processing. The typical target echo features as discussed earlier are present, with the addition of two new dominant echoes. The first, labelled G, is the echo from the sail of the submarine where its representative airfoil shape is shown in the inset of Figure 9(a). This shape gives rise to dominant echoes for non-tail facing aspect angles (from 0° to 90°, and from 270° to 360°). The maximum response from the sail occurs when the sides of the sail are beam aspect ($\pm 20°$ from the perpendicular direction), which can be seen in the spectrogram with label H. The consistent dominant echo of the sail over many aspect angles gives rise to the high amplitude (and clearly defined) return in the tomographic images for both BPA approaches, with the distinctive sail shape represented in the images.

It may be said that the weaker susceptibility to effects from strong specular reflections allows the 2DIFT BPA approach to image the outline of the GenSub model slightly better than the polar BPA approach.

3.3 Discussion

The foregoing examples highlight a number of issues that should be addressed in any practical sonar tomographic imaging system:

1. Shorter duration transmitted pulses and matched filtering are important, which can produce sharper projections and hence better image resolution.

2. Adequate pre-processing is required to reduce possible interference by multiple internal reflections or creeping surface waves around the object and to compensate for any translational motion of the target.

3. In this work, workarounds have been used to reduce the effects of signal characteristics which are beyond the scope of the current theory, such as single or multiple specular reflections and obscuration effects. However, a tomographic imaging theory

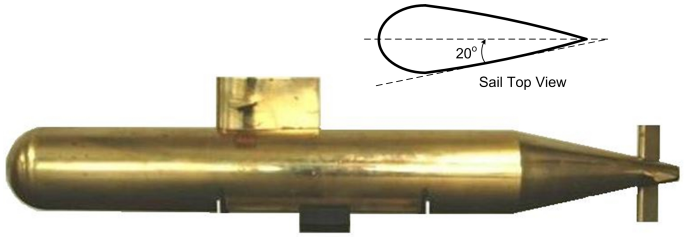

(a) A brass model of a generic submarine (GenSub)

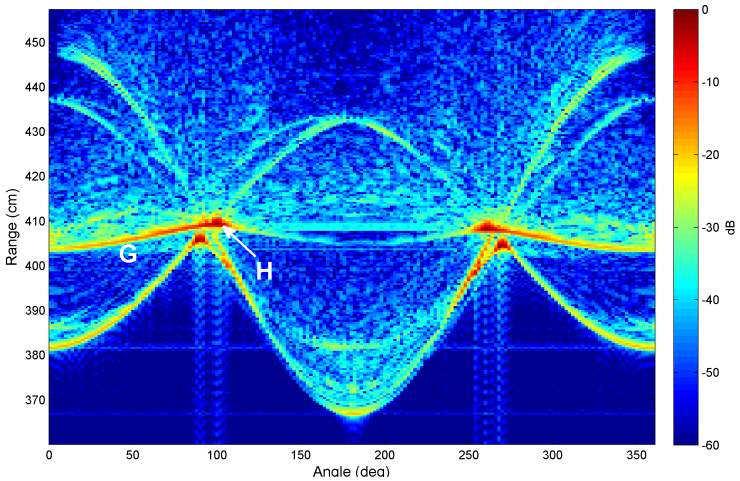

(b) Down-range profiles with attenuation applied

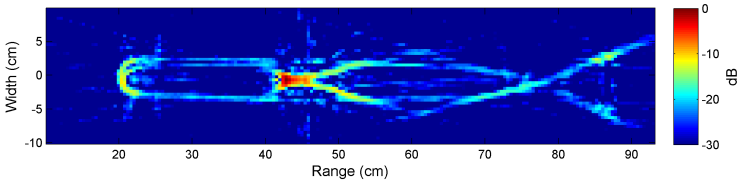

(c) Tomographic image - Polar BPA

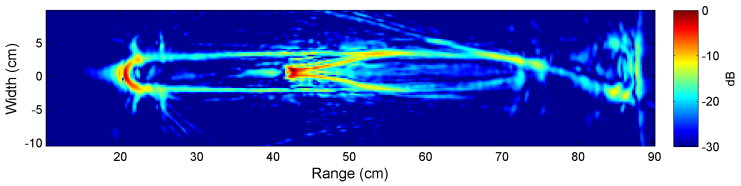

(d) Tomographic image - 2DIFFT BPA

Figure 9: *Experimental results for the GenSub model*

more suited to reflective scattering would be ideal, and will be the topic of a future research report.

3.3.1 Validation of the scattering model

The images shown in Figures 4 and 8 are of very similar quality, except for the weak appearance of some undesirable additional features in Figure 8 caused by the real effects of propagation resonances, and the fact that for the data of Figure 8 the target is suspended by hooks, which are not modelled in Figure 4. This excellent agreement indicates a very high fidelity of the scattering model employed in this work, demonstrating it as a very useful as tool for our further research work on sonar imaging and sonar target classification.

3.3.2 Performance with limited coverage of object aspect

Another aspect of performance of the two BPA approaches that may be of interest is with respect to performance when angular coverage, or bandwidth, is limited. The images presented so far have used projections from one complete cycle of object rotation, which is twice the minimum requirement. In the following, we show how the BPA approaches compare when the data is exactly one half cycle of rotation and only a quarter of a cycle. The results are in Figures 10 and 11 respectively.

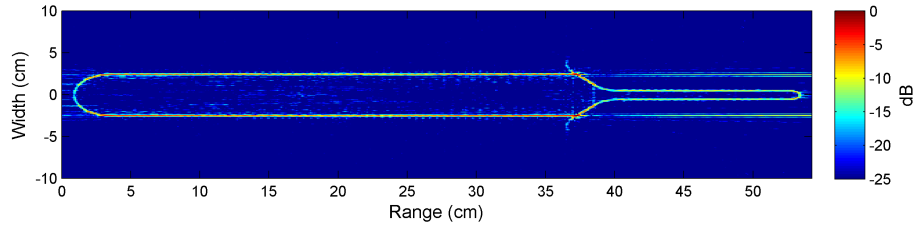

(a) Tomographic image, with the polar BPA

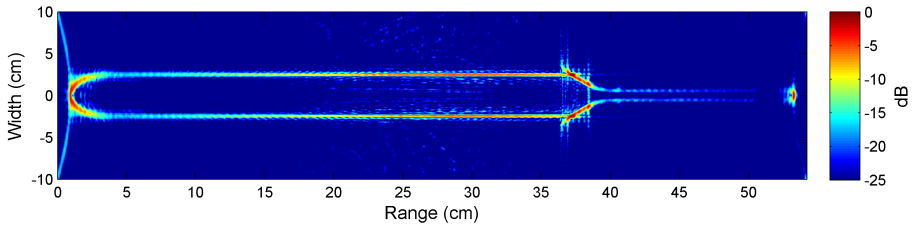

(b) Tomographic image, with the 2DIFT BPA

Figure 10: *Tomographic images using the simulated short pulse for aspects from* 0° *to* 180°

It can be seen that results in Figure 10 are very similar to those in Figure 3, except that the images are slightly sharper in Figure 3 where double the amount of data is used.

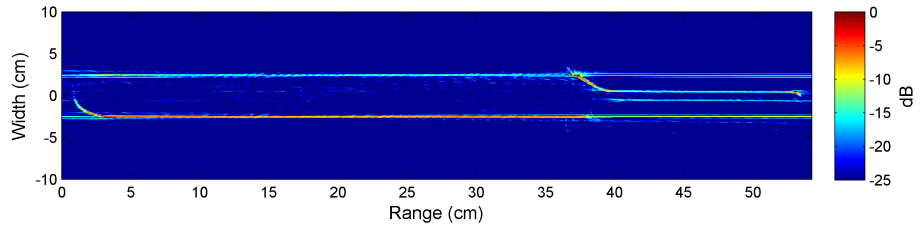

(a) Tomographic image, with the polar BPA

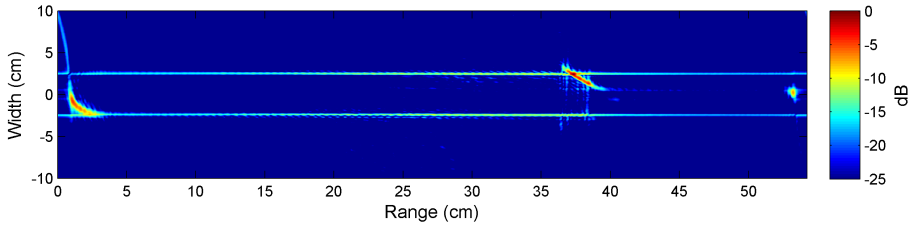

(b) Tomographic image, with the 2DIFT BPA

Figure 11: *Tomographic images using the simulated short pulse for aspects from* 0° *to* 90°

However, when only a quarter of a cycle is available, only half of the target is imaged, as seen in Figure 11, which is expected. The usefulness of these 'partial images' probably depends on the particular application.

In terms of computational cost, the polar BPA approach is slightly more expensive, but only by an extra constant factor which depends on the methodology of numerical implementation. Both approaches require an order of $N \log N$ floating point operations where N is the number of samples in each projection.

4 Conclusion

Sonar tomography is potentially a very useful technology. We have produced images with promising quality for several small objects ensonified at high frequency in a controlled laboratory environment from both experimental data and high-fidelity simulated data. We have explored and compared the performances of two back projection algorithms used in the tomographic processing and found that the two approaches are complementary, which may be combined for further improvement.

Furthermore, we discussed the data processing requirement for the sonar system, which depends on how much resolution can be achieved in the pulse compression setup of the system and the related requirement of sampling in angle (or aperture). A minimum of half a cycle of data is required for a complete tomographic image of the target. However, we also investigated how tomographic processing performs when data from only a limited

range of aspect angles is available, and found that potentially useful partial images can still be formed, for the range of aspects available.

Future works may include the following areas: (i) a development of a real-time sonar imaging prototype system; (ii) further research on better pulse compression techniques, which will directly impact achievable image resolution; and (iii) other signal pre-processing techniques to improve projections. On a more theoretical perspective, our works may also include: (i) a tomographic imaging theory more suited to reflective scattering; (ii) an extension to 3D tomography, and (iii) studies on automatic classification of sonar targets based on tomographic images.

Acknowledgements

The authors would like to sincerely thank Dr. Mark Readhead of MOD, DSTO Eveleigh for his thorough and constructive review, Dr. Andrew Shaw (RLMR), Dr. David Liebing (RLASW), Dr. Leigh Powis (HAAR), Mr. Chris Gillard (HSSP) and Mr. Stuart Sutherland (HUST) for their support of this cross-divisional research project. We also thank Mr. Duc Huynh for his brief contribution in the early stages of this work.[7]

References

1. Ferguson, B., Wyber, R., (2005) Application of acoustic reflection tomography to sonar imaging, *J. Acoust. Soc. Am.*, vol. 117 (5), pp.2915-28.

2. Ferguson, B., Wyber, R., Mapping the acoustic reflectivity of underwater objects using reconstructive tomography, *OCEANS 2008*, pp.1-7.

3. Doisy, Y., (1988) Application of Tomographic Reconstruction to Target Identifiction, *Undersea Defence Technology '88*, London, pp.433-8.

4. Pidsley, P.H., Smith, R.A., Davies, G.L., (1995) Reconstruction of sonar images using computerized tomography, *IEE Colloquium on Recent Developments in Radar and Sonar Imaging Systems*, 4/1-9.

5. Kak, A., Slaney, M., (1987) *Principles of Computerised Tomographic Imaging*, IEEE Press.

6. Scudder, H.J., (1978) Introduction to Computer Aided Tomography, *IEEE Transaction*, Vol. 66.

7. Hermann, G.T., (1980) *Image Reconstruction From Projections: Fundamentals of Computerized Tomography*, Academic Press.

8. Natterer, F., (1986) *Mathematics of Computerized Tomography*, John Wiley and Son.

9. Hein, A., (2004) *Processing of SAR Data: Fundamentals, Signal Processing, Interferometry*, Springer.

10. Tait, P., (2005) Introduction to Radar Target Recognition, *IEE Radar, Sonar and Navigation*, Series 18.

11. Baker, B.B. and Copson, E.T., (1939) *The Mathematical Theory of Huygens' Principle*, Oxford University Press, London.

[7] Mr. Duc Huynh is currently a Research Fellow in the Department of Electronic Engineering, La Trobe University.

THIS PAGE IS INTENTIONALLY BLANK

DEFENCE SCIENCE AND TECHNOLOGY ORGANISATION DOCUMENT CONTROL DATA	1. CAVEAT/PRIVACY MARKING

2. TITLE	3. SECURITY CLASSIFICATION
A Detailed Study of Sonar Tomographic Imaging	Document (U) Title (U) Abstract (U)
4. AUTHORS	5. CORPORATE AUTHOR
H.T. Tran, B. Nguyen, R. Melino, and S. Wood	Defence Science and Technology Organisation PO Box 1500 Edinburgh, South Australia 5111, Australia

6a. DSTO NUMBER	6b. AR NUMBER	6c. TYPE OF REPORT	7. DOCUMENT DATE
DSTO–RR–0394	015–647	Research Report	August, 2013

8. FILE NUMBER	9. TASK NUMBER	10. TASK SPONSOR	11. No. OF PAGES	12. No. OF REFS
2011/1127170/1	07/366		23	11

13. URL OF ELECTRONIC VERSION	14. RELEASE AUTHORITY
`http://www.dsto.defence.gov.au/publications/scientific.php`	Chief, Maritime Operations Division

15. SECONDARY RELEASE STATEMENT OF THIS DOCUMENT

Approved for Public Release

OVERSEAS ENQUIRIES OUTSIDE STATED LIMITATIONS SHOULD BE REFERRED THROUGH DOCUMENT EXCHANGE, PO BOX 1500, EDINBURGH, SOUTH AUSTRALIA 5111

16. DELIBERATE ANNOUNCEMENT

No Limitations

17. CITATION IN OTHER DOCUMENTS

No Limitations

18. DSTO RESEARCH LIBRARY THESAURUS

Tomography, Underwater Acoustics, Active Sonar, Target Imaging, Target Scattering

19. ABSTRACT

Sonar tomography is a technique to obtain a two-dimensional image of an underwater object using a sequence of one-dimensional images, or 'projections', of the object of interest. We discuss sonar tomography in a detailed manner and compare the performance of two important 'back-projection algorithms' commonly used in tomography. The two processing techniques are applied to the imaging of relatively small underwater objects using high sonar frequencies, making use of simulated and experimental data. We also discuss system requirements, as well as the similarities and differences with radar applications. Ultimately, the performance of this underwater object imaging technique is determined by the availability of sufficiently high resolution projections and/or sufficient coverage in object aspect.